Manipulating charge density wave order in monolayer $1T$-$TiSe_2$ by strain and charge doping: A first-principles investigation

M. J. Wei,[1,2] W. J. Lu,[1,*] R. C. Xiao,[1,2] H. Y. Lv,[1] P. Tong,[1] W. H. Song,[1,†] and Y. P. Sun[1,3,4]

[1]*Key Laboratory of Materials Physics, Institute of Solid State Physics, Chinese Academy of Sciences, Hefei 230031, China*

[2]*University of Science and Technology of China, Hefei 230026, China*

[3]*High Magnetic Field Laboratory, Chinese Academy of Sciences, Hefei 230031, China*

[4]*Collaborative Innovation Center of Microstructures, Nanjing University, Nanjing 210093, China*

(Received 15 June 2017; published 3 October 2017)

We investigate the effects of the in-plane biaxial strain and charge doping on the charge density wave (CDW) order of monolayer $1T$-$TiSe_2$ by using the first-principles calculations. Our results show that the tensile strain can significantly enhance the CDW order, while both compressive strain and charge doping (electrons and holes) suppress the CDW instability. The tensile strain may provide an effective method for obtaining higher CDW transition temperature on the basis of monolayer $1T$-$TiSe_2$. We also discuss the potential superconductivity in charge-doped monolayer $1T$-$TiSe_2$. Controllable electronic phase transition from the CDW state to the metallic state or even the superconducting state can be realized in monolayer $1T$-$TiSe_2$, which makes $1T$-$TiSe_2$ possess a promising application in controllable switching electronic devices based on CDW.

DOI: 10.1103/PhysRevB.96.165404

I. INTRODUCTION

Layered transition metal dichalcogenides (TMDs) have received wide-spreading attention, due to a variety of characteristic physical properties, such as charge density wave (CDW) and superconducting state [1–4]. The CDW and superconductivity are two fundamental collective quantum phenomena, and both arise from electronic instabilities in condensed matter physics. The interplay between the two has been widely investigated, however, the idea that CDW order competes and even coexists with superconductivity remains a long-standing enigma. In cuprates, the competition was directly observed in the CuO_2 monolayer atop a cuprate by scanning tunneling microscope measurements, which has provided clear evidence of spatial separation between the nodal CDW and the nodeless superconducting gap functions [5]. However, in many TMDs, it has been observed that incommensurate/nearly commensurate CDW (ICCDW/NCCDW) order can coexist with superconductivity through the formation of CDW domain walls [6–10].

Below the CDW transition temperature, the lattice distorts simultaneously accompanied with the redistribution of charge and the abrupt change of electronic transport properties, which might open new potential applications in optoelectronic and quantum information processing devices [11–14]. For practice applications, the room temperature ultrathin CDW materials are desirable. Previous experimental studies showed that reducing the thicknesses of the CDW materials can effectively tune the CDW transition temperature. For example, CDW transition temperature of $1T$-TaS_2 is shifted to lower temperature with the reduction of thickness and then disappears at critical thickness [15]. Xi *et al*. have reported that the CDW transition temperature of $2H$-$NbSe_2$ is enhanced from 33 K in the bulk to 145 K in the monolayer [16]. Recently, Chen *et al*. demonstrated that the CDW transition temperature of $1T$-$TiSe_2$ increases from 200 K in the bulk to 230 K in the monolayer [17,18]. To the best of our knowledge, the CDW transition temperature of monolayer $1T$-$TiSe_2$ is comparatively closer to the room temperature than that of other monolayer TMD materials. Hence, the monolayer $1T$-$TiSe_2$ provides an ideal platform for obtaining the CDW phase with higher transition temperature even above room temperature. This motivates us to search for methods to tune the CDW order of the monolayer $1T$-$TiSe_2$.

The ultrathin $1T$-$TiSe_2$ materials are often prepared on substrate, and the effects of the substrate-induced strain are inevitable, which offers opportunities for tuning CDW order in experiments [19,20]. Meanwhile, charge doping has also an important impact on the CDW transition [7,9]. In this work, we focus on the effects of the strain and charge doping on the CDW order in monolayer $1T$-$TiSe_2$ by using the first-principles calculations. Our results show that the tensile strain can enhance the CDW order, while the compressive strain and charge doping suppress it. The CDW gap increases with the increase of tensile strain, while the compressive strain reduces CDW gap and it undergoes a semiconductor-metal transition at 6% compressive strain. Furthermore, we discuss that the superconductivity with superconducting transition temperature T_C of 7.3–0.3 K can be introduced by electron/hole doping.

II. COMPUTATIONAL DETAILS

The first-principles calculations were performed using the QUANTUM ESPRESSO package [21] with generalized gradient approximation according to the Perdew-Burke-Ernzerhof (PBE) [22] functional. The ultrasoft pseudopotentials were used to describe the interaction between electrons and ionic cores [23]. The valence electrons were simulated by the plane wave method. The energy cutoff of 80 Ry (800 Ry) was chosen for the wave functions (charge density) basis. In order to simulate the monolayer, at least 18 Å of vacuum layer was introduced. The Brillouin zone (BZ) was sampled on a

*wjlu@issp.ac.cn

†whsong@issp.ac.cn

 ©2017 American Physical Society

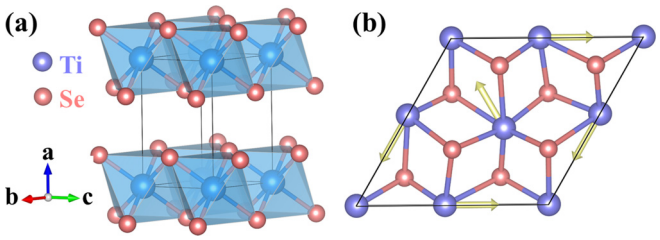

FIG. 1. Crystal structures of bulk $1T$-$TiSe_2$ for (a) normal phase at room temperature and (b) $2 \times 2 \times 1$ CDW phase at low temperature. Yellow arrows display the displacement directions of Ti atoms from the high symmetry positions of the undistorted $1T$ structure. Ti and Se atoms are denoted by blue and red balls, respectively.

$16 \times 16 \times 1$ mesh of **k** points. The total energy and electron charge density were calculated by the Fermi-Dirac smearing method. Except otherwise specified, a smearing parameter of $\sigma = 0.005$ Ry was used. Using density functional perturbation theory (DFPT) [24], phonon dispersion curves were calculated with $8 \times 8 \times 1$ **q** points for the undistorted monolayer structure. Denser $32 \times 32 \times 1$ mesh of **k** points were employed for the electron-phonon coupling calculations. For a better agreement with the experimental results, the LDA + U method with the value $U = 3.9$ eV [25] and spin-orbit interactions were considered in the electronic structure calculations. Since the spin-orbit coupling effect is less important in describing the vibrational properties [26,27], the calculation of phonon dispersion was carried out neglecting this effect. The biaxial strain was simulated by changing the lattice constant a_0, and the strength of strain was defined as $\varepsilon = (a - a_0)/a_0 \times 100\%$, for which the positive (negative) value represents the tensile (compressive) strain. For the study of charge doping effects, hole doping was modeled by removing electrons from the system, while the electron doping by increasing electrons into the system, in company with a compensating uniform negative background for hole doping and positive background for electron doping. For each doping concentration, atomic positions were relaxed with fixing the lattice parameters of the undoped monolayer $1T$-$TiSe_2$.

III. RESULTS AND DISCUSSION

Bulk $1T$-$TiSe_2$ exhibits a layered structure with the space group $P\bar{3}m1$, where adjacent layers are held together by van der Waals forces and each Ti atoms are surrounded by the nearest six Se atoms, constituting an octahedron, as illustrated in Fig. 1(a). The monolayer $1T$-$TiSe_2$ can be obtained by exfoliating the bulk $1T$-$TiSe_2$ or grown by molecular beam epitaxy [11,17]. Below ~230 K, the monolayer $1T$-$TiSe_2$ undergoes a $2 \times 2 \times 1$ commensurate CDW (CCDW) transition [17], so primitive cell lattice doubles as displayed in Fig. 1(b), and the corresponding BZ shrinks to half of that of the undistorted monolayer $1T$-$TiSe_2$.

When the bulk is thinned to the monolayer, the strain can be an effective method to manipulate the properties of materials. Hence, we first investigate the evolution of the CDW order in monolayer $1T$-$TiSe_2$ under the in-plane biaxial compressive and tensile strains. In order to comprehend the stability of

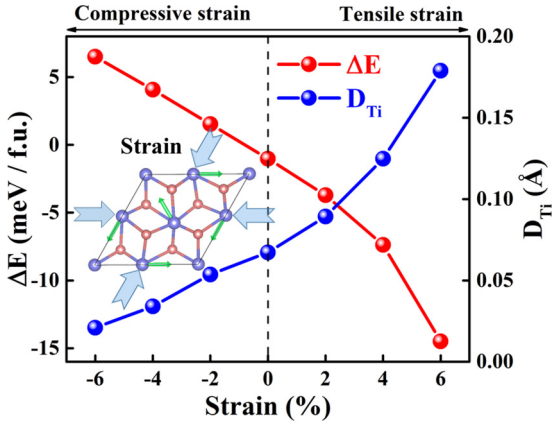

FIG. 2. CDW formation energy ΔE per formula unit (left) and average displacements of Ti atoms from the high symmetry positions of the undistorted $1T$ structure (right) as a function of biaxial strain. The inset shows the biaxial compressive strain on the monolayer $1T$-$TiSe_2$ in the CDW phase.

CDW order from an energy perspective, the CDW formation energy ΔE is defined as

$$\Delta E = E_{\mathrm{CDW}} - E_{1T}, \tag{1}$$

where E_{CDW} and E_{1T} are the total energies of the relaxed CDW structure and the undistorted $1T$ structure. Meanwhile, the CDW phase transitions can be ascribed to the results of spontaneous symmetry breaking, which involves atomic displacements, as shown in Fig. 1(b) [17]. Hence, the average displacements of Ti atoms, D_{Ti}, have also been introduced to describe the strain and charge doping dependence of CDW order from a structural perspective. Figure 2 shows the CDW formation energy and the average displacements of Ti atoms of the monolayer $1T$-$TiSe_2$ in the CDW phase as a function of biaxial strain. When the tensile strain was applied to monolayer $1T$-$TiSe_2$, the absolute value of the formation energy gradually increases, indicating that the CDW phase becomes more stable. On the contrary, the compressive strain gradually suppresses the CDW instability. From a structural perspective, the distortion amplitude of Ti atoms is remarkably enhanced by the tensile strain, while the compressive strain weakens it. These results indicate that the biaxial compressive and tensile strain can remarkably tune the CDW order.

Figure 3 shows the electronic band structures of the monolayer $1T$-$TiSe_2$ in the CDW phase as a function of biaxial strain. For comparison, the electronic band structures without applying strain are also shown [see Fig. 3(c)]. We find that the band gap has different responses to the tensile and compressive strains. The tensile strain significantly increases the band gap, while the compressive strain reduces it. A continuously varying band gap can be achieved by strain. Therefore, such behavior leads to the transition from semiconductor to metal at 6% compressive strain, as shown in Fig. 3(a).

Recent studies show that the Fermi-surface nesting is indeed irrelevant to the formation of the CDW phase in $1T$-$TiSe_2$ [17,28], and the electron-phonon coupling is considered as a main driving force of the CDW instability [25,29–31]. The phonon calculation is proven to be an effective method to simulate the CDW instability [31–33]. The phonon instability

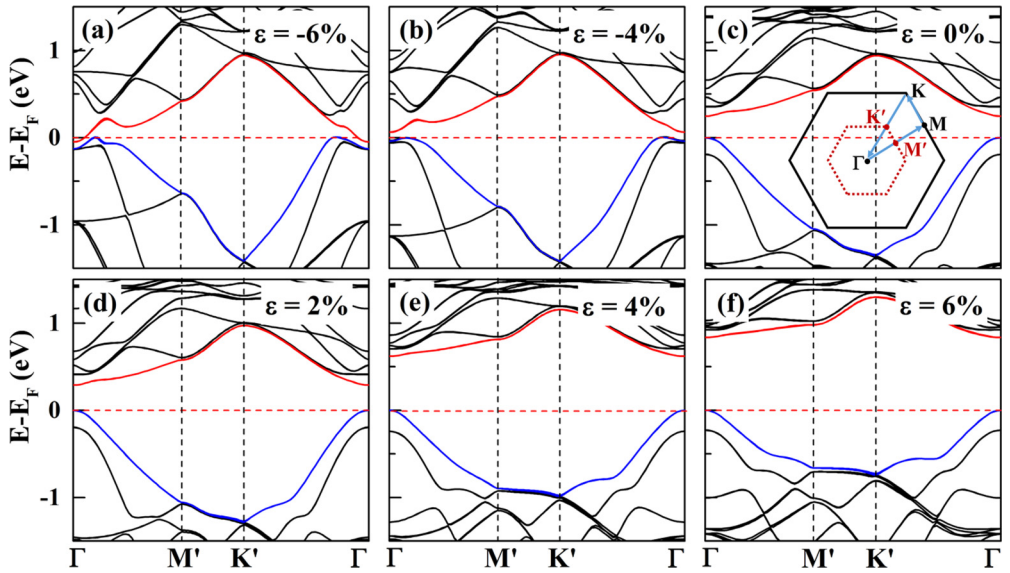

FIG. 3. Evolution of the electronic band structures of the monolayer $1T$-$TiSe_2$ in the CDW phase under biaxial strain: (a) and (b) for compressive strain, (c) without strain, and (d)-(f) for tensile strain. Blue (red) solid lines in each panel indicate the highest valence band (the lowest conduction band). The top of the valence band is set to zero. The inset in (c) shows the BZs of the monolayer $1T$-$TiSe_2$. Black solid line represents the BZ of the normal phase and red dotted line represents the folded BZ due to CDW phase transition.

of high-symmetry structure can be described as a result of the CDW distortion: Close to but higher than the CDW transition temperature, the phonon frequencies in the vicinity of the CDW vector $\mathbf{q}_{\mathrm{CDW}}$ soften but do not go to zero, while the phonon frequencies become imaginary below the CDW transition temperature [31–33]. The occurrence of imaginary phonon frequencies implies that the structure is unstable. A structure is considered to be stable when the calculated frequencies of all phonon modes are positive. Figure 4(c) shows the calculated phonon dispersion curves of monolayer $1T$-$TiSe_2$. We find that the imaginary/softened acoustic mode at the M point associated with the $2 \times 2 \times 1$ CDW instability of monolayer $1T$-$TiSe_2$ becomes more dynamically unstable than that of the bulk (data not shown here), indicating that the CDW order of monolayer $1T$-$TiSe_2$ is more robust than that of the bulk. This is qualitatively consistent with the experimental observations that reducing thickness increases CDW transition temperature [17,18,30].

In order to further understand the evolution of the CDW order under the biaxial strain, we calculated the phonon dispersion curves under different biaxial strains. Figures 4(a)–4(c) show that the compressive strain can enhance the phonon frequencies and reduce the area of instability at the CDW vector $\mathbf{q}_M$. When the compressive strain of 6% is applied, the previous imaginary frequencies at the M point become positive [see Fig. 4(a)], indicating that the normal phase becomes stable against CDW transition. Figures 4(c)–4(f) show that the tensile strain can reduce the phonon frequencies and largely expand the area of instability at the CDW vector $\mathbf{q}_M$. When the tensile strain of 6% is applied, additional imaginary acoustic branches are introduced [see Fig. 4(f)], indicating that the larger tensile strain results in the structure phase transition in monolayer $1T$-$TiSe_2$. We can conclude that the tensile strain can enhance the CDW order, while the compressive strain suppresses it. It is expected that the tensile strain could further increase the CDW transition temperature of monolayer $1T$-$TiSe_2$. In addition, we note that there are small imaginary frequencies close to the Γ point in Figs. 4(a) and 4(b), which are consistent with an instability due to the long-wavelength transverse waves [34,35]. Grain boundaries or ripples and other defects are capable of fixing such small instability [34–36].

In order to qualitatively simulate the influence of temperature on CDW order, the temperature dependence of phonon dispersion curves were calculated by changing the Fermi-Dirac smearing factor σ. This parameter takes on a physical meaning to directly reflect the electronic temperature of the system [37]. The disappearance of the imaginary phonon frequencies at the M point in phonon dispersion curves means that the CDW instability is eliminated by increasing σ. Figure 4(c) shows the phonon dispersion curves of the unstrained monolayer $1T$-$TiSe_2$ with different σ. The imaginary/softened acoustic branches show significant dependence on the electronic temperature. As the electronic temperature increases, the area of the instability reduces and disappears at $\sigma \sim 0.007$–0.008 Ry. According to the method proposed by Duong *et al.* [37], the CDW transition temperatures T_{CDW} can be obtained by fitting the smearing electron temperature-phonon frequencies at the M point based on the following equation [37]:

$$\omega_M(T) = \omega_0 * (T - T_{\mathrm{CDW}})^{\delta}. \quad (2)$$

Figures 5(a) and 5(b) show the fitted smearing electron temperature dependence of phonon frequencies at the M point and the obtained T_{CDW} under tensile strain, respectively. The fitting parameters are listed in Table I. As the tensile strain increases, the T_{CDW} becomes higher, further demonstrating that the tensile strain can enhance the CDW order. We can conclude that the control of strain allows us to manipulate the CDW transition, which may open a promising application in the future to construct controllable switching electronic devices

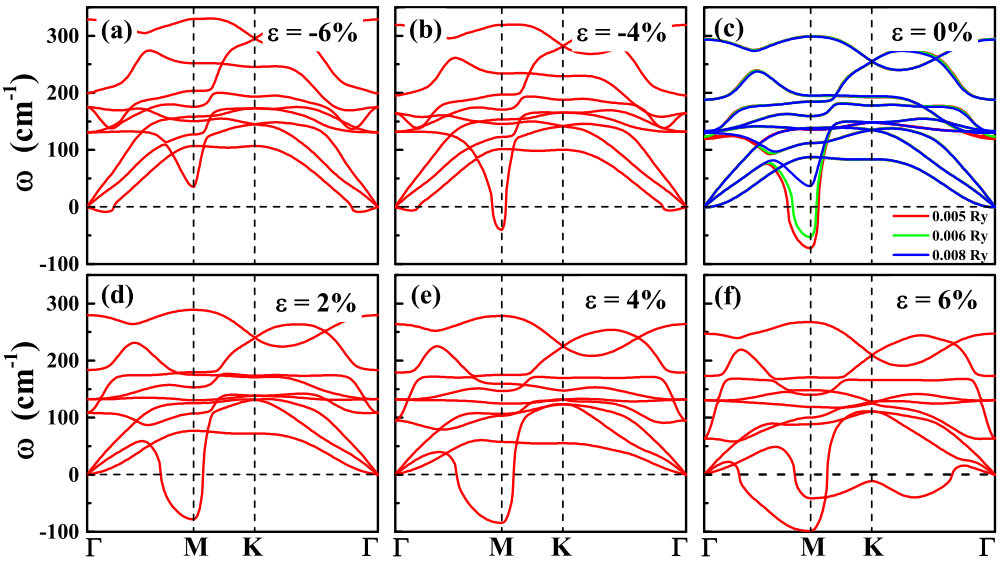

FIG. 4. Evolution of the phonon dispersion curves of monolayer $1T$-$TiSe_2$ in the normal phase under the biaxial strain: (a) and (b) for compressive strain, (c) without strain, and (d)-(f) for tensile strain. Colored curves in (c) stand for phonon dispersion curves with different values of electronic smearing parameter σ.

based on CDW. Note that the real temperature of the crystal should include not only the temperature of the electron but also of the lattice, hence the calculated electron temperature cannot directly represent the real physical temperature and needs to be further amended. Despite the fact that the obtained T_{CDW} is not accurate enough numerically, it can correctly describe the evolution of the CDW transition under the strain.

Charge carrier doping can be easily introduced in experiments, such as gate-controlled Li ion intercalation, electric-field effect, and photoexcitation, which has been successfully applied to manipulate the CDW transition [7,9,38,39]. Here, we also investigated the effect of the charge doping on the CDW order in monolayer $1T$-$TiSe_2$. Figures 6(a) and 6(b) show the calculated phonon dispersion curves of monolayer $1T$-$TiSe_2$ with different doping concentrations. They indicate that both electron and hole doping can suppress the CDW instability. In order to more clearly see the evolution of the suppression of the CDW transition by charge doping, a series of phonon dispersion curves of monolayer $1T$-$TiSe_2$ and the average distortion of Ti atoms in CDW-phase $TiSe_2$ under different doping concentrations were calculated. The phonon frequencies at the M point and the average distortion of Ti atoms were summarized in Fig. 6(c). One can see that the average distortion of Ti atoms gradually becomes smaller and eventually tends to zero with the increase of doping concentrations. When the doping concentration is above $n = 0.165$ electrons/f.u. or $n = 0.055$ holes/f.u., the previous imaginary frequencies at the M point become positive, which indicates the doped monolayer $1T$-$TiSe_2$ with the normal phase becomes completely stable. We can conclude that both electron and hole doping are harmful to stabilize the CDW order in the system. Hence, if one wants to obtain high CDW transition temperature in monolayer $1T$-$TiSe_2$, charge doping needs to be prohibited.

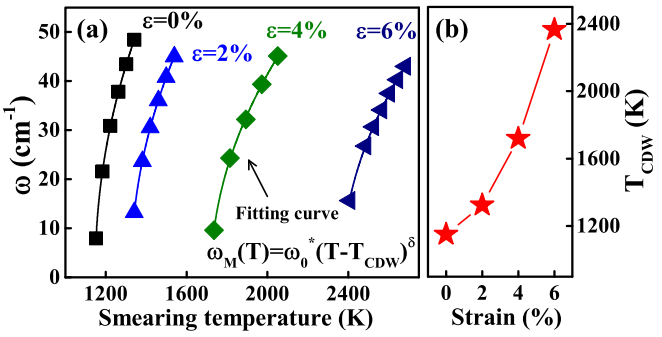

FIG. 5. (a) Phonon frequencies of softened acoustic mode at the M point as a function of the electronic temperature under tensile strain. The solid lines are fitted by Eq. (2). (b) Fitted CDW transition temperatures T_{CDW} under tensile strain.

Superconductivity can be induced in $1T$-$TiSe_2$ when the CCDW phase is suppressed by applying electric-field [9], pressure [8], or through Cu intercalation [10]. For example, in a gate-tuned thin film of pure $1T$-$TiSe_2$, the CDW transition temperature quickly decreases with increasing the doping concentration and the superconducting phase emerges from 0 K at $n = 1.2 \times 10^{14}\text{cm}^{-2}$ and reaches the maximal T_C of $\sim$3 K at $n = 7.5 \times 10^{14}\text{cm}^{-2}$, for which the CDW signal becomes undetectable [9]. Similar superconducting phase diagrams have also been observed in Cu_xTiSe_2 [10]. These studies also suggested that the emergence of an ICCDW phase through the formation of domain walls may play a significant

TABLE I. Fitting parameters of smearing electron temperature dependence of phonon frequencies at the M point under tensile strain in Fig. 5(a).

Strain	T_{CDW}(K)	ω_0(cm^{-1})	δ
0%	1147	3.89	0.479
2%	1324	3.37	0.483
4%	1720	2.48	0.500
6%	2366	2.61	0.487

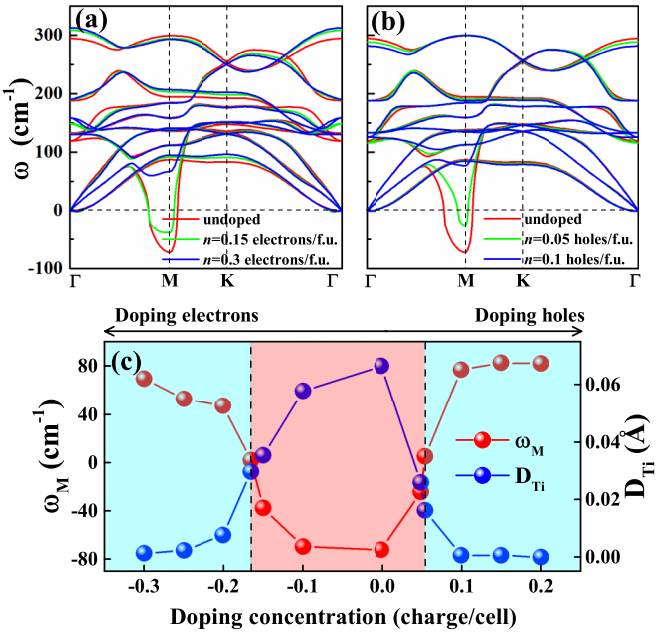

FIG. 6. Phonon dispersion curves for (a) electron-doped and (b) hole-doped monolayer $1T$-$TiSe_2$ under some typical doping concentrations. For comparison, undoped monolayer $1T$-$TiSe_2$ is also shown, which is depicted as red solid lines. (c) The phonon frequencies at the M point (left) and the average displacements of Ti atoms from the high symmetry positions of the undistorted $1T$ structure (right) as a function of doping concentration. The region decorated with red color stands for the CDW phase.

role in the development of superconductivity [8–10]. As the CCDW phase is suppressed, the CDW domains gradually shrink and the ICCDW grows in interdomain regions, which can be considered as conducting channels to induce the metallic state [40]. Once the metallic interdomain regions are percolated, superconductivity can emerge. While we are not able to directly model the textured ICCDW phase, we can still qualitatively investigate the superconductivity using $1T$ structure. Here, when the CDW is completely suppressed, we estimate the T_C by using the Allen-Dynes-modified McMillan formula [41,42]:

$$T_C = \frac{\omega_{\log}}{1.2} \exp\left(-\frac{1.04(1+\lambda)}{\lambda - \mu^* - 0.62\lambda\mu^*}\right), \tag{3}$$

where the total electron-phonon coupling constant is

$$\lambda = \sum_{\mathbf{q}v} \lambda_{\mathbf{q}v} = 2\int \frac{\alpha^2 F(\omega)}{\omega} d\omega. \tag{4}$$

The Coulomb pseudopotential μ^* is generally assumed to 0.1 [28,43,44]. The logarithmic average frequency of $\omega_{\log}$ is defined as

$$\omega_{\log} = \exp\left(\frac{2}{\lambda}\int \frac{d\omega}{\omega}\alpha^2 F(\omega)\log\omega\right), \tag{5}$$

with the Eliashberg spectral function,

$$\alpha^2 F(\omega) = \frac{1}{2\pi N(E_F)} \sum_{\mathbf{q}v} \delta(\omega - \omega_{\mathbf{q}v}) \frac{\gamma_{\mathbf{q}v}}{\hbar\omega_{\mathbf{q}v}}, \tag{6}$$

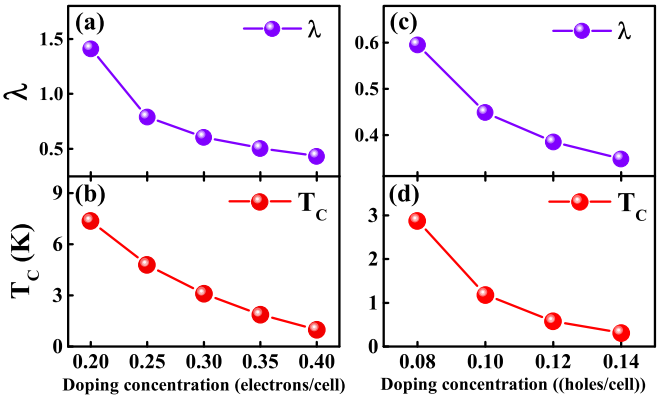

FIG. 7. Calculated λ and T_C of monolayer $1T$-$TiSe_2$ under (a) and (b) electron doping, and (c) and (d) hole doping.

where $N(E_F)$ is the density of states at E_F, and $\gamma_{\mathbf{q}v}$ is the phonon linewidth.

Figures 7(b) and 7(d) show that the doped monolayer $1T$-$TiSe_2$ could be superconducting and the T_C decreases monotonously from 7.3 K (2.8 K) at 0.2 electrons/f.u. (0.08 holes/f.u.) to 0.9 K (0.3 K) at 0.4 electrons/f.u. (0.14 holes/f.u.). We try to understand the evolution: As the CDW instability is just suppressed and the system enters into the normal phase, the original imaginary frequency ω at the M point becomes a small positive value. The small positive ω in Eq. (4) can lead to a large λ, resulting in the high T_C. However, according to Fig. 6(c), both electron doping and hole doping make the phonon spectra harden, which leads to the reduction of λ and is not beneficial to the superconductivity [Figs. 7(a) and 7(c)]. As a result, T_C decreases monotonously with the increase of the charge doping concentration. Our results are in qualitative agreement with experiments, although in experiments the domelike shape of T_C versus doping concentration emerges [9]. This discrepancy between the calculated and measured T_C could be due to neglecting textured ICCDW structure in the calculations.

IV. CONCLUSIONS

In conclusion, we have studied the effects of the biaxial strain and charge doping on the CDW order of monolayer $1T$-$TiSe_2$ by the first-principles calculations. We found that the tensile strain can effectively enhance the CDW order. The results indicate that the CDW transition temperature of monolayer $1T$-$TiSe_2$ grown on substrates with large lattice constants can be enhanced. The compressive strain and the charge doping can suppress the CDW order. At the 6% compressive strain or at the doping concentrations of 0.165 electrons/f.u. and 0.055 holes/f.u., the CDW instability is completely eliminated. When the CDW instability is suppressed by charge doping, the superconductivity with T_C of 7.3–0.3 K can be introduced by electron/hole doping. Controllable electronic phase transition from the CDW state to the metallic state or even the superconducting state can be realized in monolayer $1T$-$TiSe_2$,

which makes $1T$-$TiSe_2$ possess a promising application in controllable switching electronic devices based on CDW.

ACKNOWLEDGMENTS

This work was supported by the National Key R&D Program of China under Contract No. 2016YFA0300404, the National Nature Science Foundation of China under Contracts No. 11674326, No. 11774351, No. 11704001, and No. U1232139, Key Research Program of Frontier Sciences of CAS (QYZDB-SSW-SLH015), and Hefei Science Center of CAS (2016HSC-IU011). The calculations were partially performed at the Center for Computational Science, CASHIPS.

[1] R. A. Klemm, *Layered Superconductors* (Oxford University Press, Oxford, 2012), Vol. 1.
[2] R. A. Klemm, Physica C (Amsterdam) **514**, 86 (2015).
[3] J. A. Wilson and A. D. Yoffe, Adv. Phys. **18**, 193 (1969).
[4] M. Chhowalla, H. S. Shin, G. Eda, L.-J. Li, K. P. Loh, and H. Zhang, Nat. Chem. **5**, 263 (2013).
[5] Y. Zhong, Y. Wang, S. Han, Y.-F. Lv, W.-L. Wang, D. Zhang, H. Ding, Y.-M. Zhang, L. Wang, and K. He, Science Bulletin **61**, 1239 (2016).
[6] B. Sipos, A. F. Kusmartseva, A. Akrap, H. Berger, L. Forro, and E. Tutis, Nat. Mater. **7**, 960 (2008).
[7] Y. Yu, F. Yang, X. F. Lu, Y. J. Yan, Y.-H. Cho, L. Ma, X. Niu, S. Kim, Y.-W. Son, D. Feng, S. Li, S.-W. Cheong, X. H. Chen, and Y. Zhang, Nat. Nanotechnol. **10**, 270 (2015).
[8] Y. I. Joe, X. M. Chen, P. Ghaemi, K. D. Finkelstein, G. A. de la Pena, Y. Gan, J. C. T. Lee, S. Yuan, J. Geck, G. J. MacDougall, T. C. Chiang, S. L. Cooper, E. Fradkin, and P. Abbamonte, Nat. Phys. **10**, 421 (2014).
[9] L. J. Li, E. C. T. O'Farrell, K. P. Loh, G. Eda, B. Özyilmaz, and A. H. Castro Neto, Nature **529**, 185 (2016).
[10] A. Kogar, G. A. de la Pena, S. Lee, Y. Fang, S. X.-L. Sun, D. B. Lioi, G. Karapetrov, K. D. Finkelstein, J. P. C. Ruff, P. Abbamonte, and S. Rosenkranz, Phys. Rev. Lett. **118**, 027002 (2017).
[11] P. Goli, J. Khan, D. Wickramaratne, R. K. Lake, and A. A. Balandin, Nano Lett. **12**, 5941 (2012).
[12] D. Mihailovic, D. Dvorsek, V. V. Kabanov, J. Demsar, L. Forró, and H. Berger, Appl. Phys. Lett. **80**, 871 (2002).
[13] N. Ogawa and K. Miyano, Appl. Phys. Lett. **80**, 3225 (2002).
[14] J. Khan, C. M. Nolen, D. Teweldebrhan, D. Wickramaratne, R. K. Lake, and A. A. Balandin, Appl. Phys. Lett. **100**, 043109 (2012).
[15] A. W. Tsen, R. Hovden, D. Wang, Y. D. Kim, J. Okamoto, K. A. Spoth, Y. Liu, W. J. Lu, Y.-P. Sun, and J. C. Hone, Proc. Natl. Acad. Sci. USA **112**, 15054 (2015).
[16] X. Xi, L. Zhao, Z. Wang, H. Berger, L. Forró, J. Shan, and K. F. Mak, Nat. Nanotechnol. **10**, 765 (2015).
[17] P. Chen, Y. H. Chan, X. Y. Fang, Y. Zhang, M. Y. Chou, S. K. Mo, Z. Hussain, A. V. Fedorov, and T. C. Chiang, Nat. Commun. **6**, 8943 (2015).
[18] P. Chen, Y. H. Chan, M. H. Wong, X. Y. Fang, M. Y. Chou, S. K. Mo, Z. Hussain, A. V. Fedorov, and T. C. Chiang, Nano Lett. **16**, 6331 (2016).
[19] S. Damjan, V. Igor, S. Petra, G. Evgeni, G. Jan, M. Tomaz, and M. Dragan, Appl. Phys. Express **7**, 103201 (2014).
[20] R. Zhao, Y. Wang, D. Deng, X. Luo, W. J. Lu, Y.-P. Sun, Z.-K. Liu, L.-Q. Chen, and J. Robinson, Nano Lett. **17**, 3471 (2017).
[21] G. Paolo, B. Stefano, B. Nicola, C. Matteo, C. Roberto, C. Carlo, C. Davide, L. C. Guido, C. Matteo, D. Ismaila, C. Andrea Dal, G. Stefano de, F. Stefano, F. Guido, G. Ralph, G. Uwe, G. Christos, K. Anton, L. Michele, M.-S. Layla, M. Nicola, M. Francesco, M. Riccardo, P. Stefano, P. Alfredo, P. Lorenzo, S. Carlo, S. Sandro, S. Gabriele, P. S. Ari, S. Alexander, U. Paolo, and M. W. Renata, J. Phys.: Condens. Matter **21**, 395502 (2009).
[22] J. P. Perdew, K. Burke, and M. Ernzerhof, Phys. Rev. Lett. **77**, 3865 (1996).
[23] D. Vanderbilt, Phys. Rev. B **41**, 7892 (1990).
[24] S. Baroni, S. de Gironcoli, A. Dal Corso, and P. Giannozzi, Rev. Mod. Phys. **73**, 515 (2001).
[25] R. Bianco, M. Calandra, and F. Mauri, Phys. Rev. B **92**, 094107 (2015).
[26] V. Chis, I. Y. Sklyadneva, K. A. Kokh, V. A. Volodin, O. E. Tereshchenko, and E. V. Chulkov, Phys. Rev. B **86**, 174304 (2012).
[27] M. J. Verstraete, M. Torrent, F. Jollet, G. Zérah, and X. Gonze, Phys. Rev. B **78**, 045119 (2008).
[28] M. Calandra and F. Mauri, Phys. Rev. Lett. **106**, 196406 (2011).
[29] M. Porer, U. Leierseder, J. M. Ménard, H. Dachraoui, L. Mouchliadis, I. E. Perakis, U. Heinzmann, J. Demsar, K. Rossnagel, and R. Huber, Nat. Mater. **13**, 857 (2014).
[30] D. L. Duong, G. Ryu, A. Hoyer, C. Lin, M. Burghard, and K. Kern, ACS Nano **11**, 1034 (2017).
[31] B. Singh, C.-H. Hsu, W.-F. Tsai, V. M. Pereira, and H. Lin, Phys. Rev. B **95**, 245136 (2017).
[32] Y. Ge and A. Y. Liu, Phys. Rev. B **82**, 155133 (2010).
[33] D. F. Shao, R. C. Xiao, W. J. Lu, H. Y. Lv, J. Y. Li, X. B. Zhu, and Y. P. Sun, Phys. Rev. B **94**, 125126 (2016).
[34] S. Cahangirov, M. Topsakal, E. Aktürk, H. Şahin, and S. Ciraci, Phys. Rev. Lett. **102**, 236804 (2009).
[35] A. J. Mannix, X.-F. Zhou, B. Kiraly, J. D. Wood, D. Alducin, B. D. Myers, X. Liu, B. L. Fisher, U. Santiago, J. R. Guest, M. J. Yacaman, A. Ponce, A. R. Oganov, M. C. Hersam, and N. P. Guisinger, Science **350**, 1513 (2015).
[36] H.Şahin, S. Cahangirov, M. Topsakal, E. Bekaroglu, E. Akturk, R. T. Senger, and S. Ciraci, Phys. Rev. B **80**, 155453 (2009).
[37] D. L. Duong, M. Burghard, and J. C. Schön, Phys. Rev. B **92**, 245131 (2015).
[38] I. Vaskivskyi, I. A. Mihailovic, S. Brazovskii, J. Gospodaric, T. Mertelj, D. Svetin, P. Sutar, and D. Mihailovic, Nat. Commun. **7**, 11442 (2016).
[39] T.-R. T. Han, F. Zhou, C. D. Malliakas, P. M. Duxbury, S. D. Mahanti, M. G. Kanatzidis, and C.-Y. Ruan, Sci. Adv. **1**, e1400173 (2015).
[40] S. Yan, D. Iaia, E. Morosan, E. Fradkin, P. Abbamonte, and V. Madhavan, Phys. Rev. Lett. **118**, 106405 (2017).
[41] P. B. Allen and R. C. Dynes, Phys. Rev. B **12**, 905 (1975).
[42] R. C. Dynes, Solid State Commun. **10**, 615 (1972).
[43] E. S. Penev, A. Kutana, and B. I. Yakobson, Nano Lett. **16**, 2522 (2016).
[44] J. Kortus, I. I. Mazin, K. D. Belashchenko, V. P. Antropov, and L. L. Boyer, Phys. Rev. Lett. **86**, 4656 (2001).